Morphology of damage occurring during decompression in a hydrogen-exposed EPDM

Ousseynou Kane Diallo, Sylvie Castagnet, Jean-Claude Grandidier, Azdine Nait- Ali

Morphology of damage occurring during decompression in a hydrogen-exposed EPDM

O. Kane Diallo, S. Castagnet, J.C. Grandidier & A. Nait-Ali
Département de Physique et Mécanique des Matériaux, Institut P' CNRS, ENSMA, Université de Poitiers, Futuroscope Cedex, France

ABSTRACT: A polymer exposed to a diffusing gas can be damaged by cavitation and/or cracking when the gas sorbed in the polymer expands faster than it desorbs out of the material. This phenomenon was reported several decades ago, but few studies aimed to quantify the morphology of cavitation damage, especially the statistics of cavity fields, and especially in hydrogen. This work addressed the time evolution of (i) cavity fields (number, size and spatial distribution) and (ii) the inflation/deflation kinetics of single cavities, in a transparent EPDM exposed to 9 MPa hydrogen pressure, saturated for 1 h and submitted to a 2.5 MPa/min gas decompression rate. Statistical analysis was based on a covariogram method applied to successive pictures taken all along the decompression test. Isotropy and time evolution of the phenomenon could be discussed at the macroscopic scale and at the morphological Representative Elementary Volume scale (REV).

1 INTRODUCTION

Ethylene-Propylene-Diene-Monomer (EPDM) elastomer is widely used in many industrial applications. EPDM exhibits excellent resistance to weather, ozone, acids and thermal degradation. These properties make it a potential material for barrier and sealing in the automotive, electrical and industrial applications. For example, EPDM can be used in the O-rings of seal equipment under high-pressure gas (CH4, H2S, H2 …). Therefore, it is important for manufacturers to investigate the influence of hydrogen on the strength properties and damage of this material (Busse et al. 1938).

Indeed, after exposure to diffusing gas for a long time, elastomer undergo internal fracture (nucleation of bubbles, forming or cracks) when the high pressure is suddenly released. This phenomenon is often referred to "explosive decompression failure" but also happens at slow decompression rates (Briscoe 1994, Yamabe 2008). Most of the reported works addressed the damage sensitivity to decompression conditions (Yamabe 2008, Jaravel 2011). From a mechanical point of view, cavitation criteria were widely inspired from purely mechanical cavitation modeling (Yamabe 2008). More recently, it was evidenced that critical pressure criteria were not relevant to depict cavitation onset in diffuso-mechanical coupled conditions (Jaravel 2013).

Damage morphology and evolution at the local scale (of a single cavity or a small number of close cavities) and at the full cavity filed scale has not been widely characterized and quantified. Interactions effects between neighboring cavities need to be highlighted too.

The aim of this study was first to investigate the evolution of a single cavity (inflection and deflection kinetics) in elastomer matrix and to look into possible interactions with its neighboring cavities. The second aim was to address the statistical evolution of cavities fields over time and over decompression conditions. A mathematical tool (covariogram method) was used for statistical analysis. The work was conducted in a transparent unfilled EPDM.

2 MATERIAL AND METHODS

2.1 *Material and sample*

This study was carried out in an unfilled EPDM, provided by Pr. Nishimura from Hydrogenius Laboratory at Kyushu University. Since this material was transparent, direct observation of the damage during decompression test was possible using visible light transmission all along the test.

Two types of test specimens were cut from molded sheets (147 × 147 × 2 mm): rectangular (30 × 8 × 2 mm) and square specimen (20 × 20 × 2 mm). They were designed considering the reduced size of the decompression chamber and the difficulty to have an optical focusing. The influence of the sample shape will be discussed later in the paper.

2.2 *Experiments*

Tests were performed in an INSTRON hydraulic tensile machine fitted with a pressure vessel allowing gas pressure up to 40 MPa, between the ambient temperature and 150°C. The door of the chamber included a central window to track damage at the optically visible scale. For safety reason related to hydrogen, the volume of the chamber was small (1.77 L with a diameter of 150 mm and length of 100 mm). More information on this device can be found in previous papers (Castagnet et al. 2002). To avoid oxygen/hydrogen mixture in the pressure cell before starting the experiment, three successive pressurization/depressurization cycles were performed by introducing nitrogen up to 1 MPa. In the present paper, all samples were initially at ambient temperature. Pressurization and decompression stages followed pressure ramps with constant pressure rates of 1 MPa/min and 2.5 MPa/min respectively. Figure 1 illustrates the pressure cycle applied to samples. Samples were clamped at one end and only guided at the other end to stay in the optical plane, without any stretching during the test. In order to estimate reproducibility, 4 samples were submitted to the same decompression conditions: 2 rectangular samples introduced at the same time in the chamber (like for any decompression condition) and 2 square samples (2 different tests). They were exposed to hydrogen gas at a maximum pressure saturation of $P_{sat} = 9$ MPa for 1 h.

After exposure, the hydrogen gas was decompressed down to the atmospheric pressure. During test, the temperature and the pressure in the vessel were recorded every second.

2.3 *Image processing*

Since the vessel was equipped with glass windows, damage onset and morphology could be tracked all along the test. It was observed under visible light transmission, using a wired light and a Sony XCD SX 90CCD camera fitted with an Avenir TV Zoom Lens 12.5–75 mm F18. There was never any visible damage in the sample during pressurization and gas saturation. Pictures were taken at a rate of one picture per second during and after decompression. The precision of detection was estimated to 26 µm i.e. the first detected cavity had a 26 µm diameter (equal to 1 pixel). The detection of the first cavity was done by image subtraction: the first picture at the beginning of decompression was subtracted to all pictures taken after this time. Time was counted from the beginning of decompression and t_{cav} was the time elapsed between the beginning of decompression and onset of the first visible cavity.

Two types of information could be extracted from image analysis during the decompression test: (i) the inflation and deflation rate of single large cavities selected at different places in the sample, and (ii) features of the full-field of cavities (number of cavities, size distribution and spatial distribution). Figure 2 illustrates the image processing previously applied to pictures. Due to the boundary layer of the sample where no cavity was detected (Jaravel et al. 2013), the processed area was reduced to a window (21 × 6 mm for the rectangular specimens and 19 × 19 mm for the square specimens). Image processing followed two steps:

– *Binarisation*: pictures were thresholded to pick out cavities as represented in Figure 2b. An erosion process was applied to remove dust or initial defects that should not be included in cavity analysis.
– *Reconstruction*: After binarisation, some cavities may have lost regular shape because of the grey level difference. A reconstruction algorithm, involving the thresholded picture and the original one, was used to restore cavities to their initial shape. This algorithm approximated cavity as a spheres.

From this reconstruction, centroids and cavity diameter could be deduced. The number of cavities

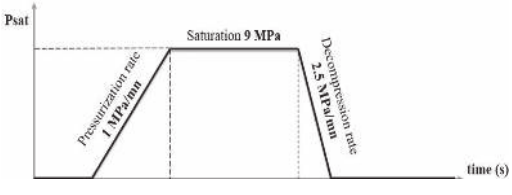

Figure 1. Loading cycle pressure of samples.

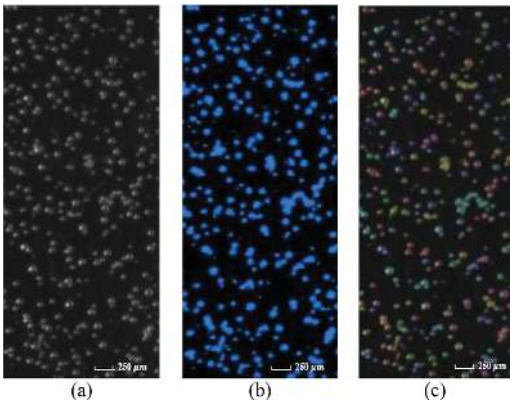

Figure 2. Image processing of sample at $P_{sat} = 9$ MPa for 1 h and decompress to atmospheric pressure at 2.5 MPa/min (a) Raw image (b) Binarisation (c) Reconstruction.

and size (average and distribution) could be plotted as a function of time. The diameter evolution of single cavities could be picked up too.

2.4 *Statistical analysis of cavity fields*

In order to quantify the spatial distribution of cavity fields and its evolution with time, a statistical analysis was applied to reconstruct pictures. Analysis was based on covariogram building (Bez 1995, Cressi 1991). In micromechanical modelling, covariograms are often used as a statistical analysis to estimate the features or mor-phological Representative Elementary Volumes (REV), from representative pictures of the initial microstructure. It is defined as the probability C(h) to encounter a cavity at distance h of another cavity along one given direction. A typical example of the obtained function C(h) is displayed in Figure 3. Several parameters could be extracted from such curves:

- At h = 0, i.e. at the center of a given cavity, the probability C(0) was equal to the global surface ratio of cavities.
- Far away from this cavity, at large h values, the probability to find another cavity became equal to a low constant value. If this asymptote value equaled the square of the surface ratio, then the distribution could be considered as homogeneous.
- In between, parameter D_c was the correlation length i.e. distance beyond which the statistical influence became negligible. It could be viewed as a morphological REV. By comparing D_c values along different directions, it was possible to get information about the anisotropy of the spatial distribution of cavities within the field. It provided information about the onset of multiple cavities populations.
- The repulsion length D_r corresponded to the average distance between 2 nearby cavities.

The method was extended here to successive pictures of the microstructure along time. One can refer to (Nait-Ali et al, in press) for more details about the method. All the above listed parameters could be tracked as a function of time during decompression.

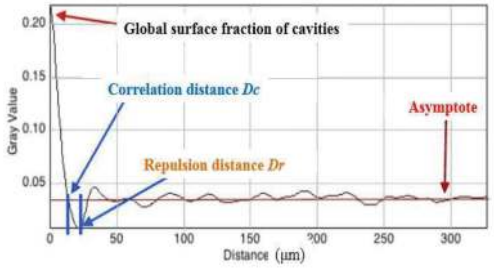

Figure 3. Example of covariogram and parameters used for statistical analysis.

3 RESULTS AND DISCUSSION

3.1 *Onset time of the first cavity*

Important information recorded during decompression tests was the onset time of the first cavity. The experimental device as well as the image processing allowed to determinate t_{cav}. It is reminded that no damage has been observed during pressurization and saturation stages consistently with the literature (Stewart, 1970).

For reproducibility requirement, the same test at P_{sat} = 9 MPa and $\dot{P}$ = 2.5 MPa/min was carried out twice, not consecutively. Firstly, the first cavity occurs after the end of decompression: t_{cav} was between 5 s and 14 s after the end of decompression for the rectangular specimens and 16 s after the end of decompression for square ones. It means that in such condition, the beginning of damage could not be governed only by the external loading: cavities appeared while all external parameters (temperature, gas pressure) were constant. After the end of decompression, there was still gas in the sample because gas diffusion was not fast enough for desorption to be completed although pressure in the chamber had returned to atmosphere. By comparing the two types of samples, the onset time of cavitation seemed to be independent on sample wideness. Secondly, cavitation only affected the center of the sample: no cavity was detected near free surfaces (Figure 4b) due to hydrogen diffusion

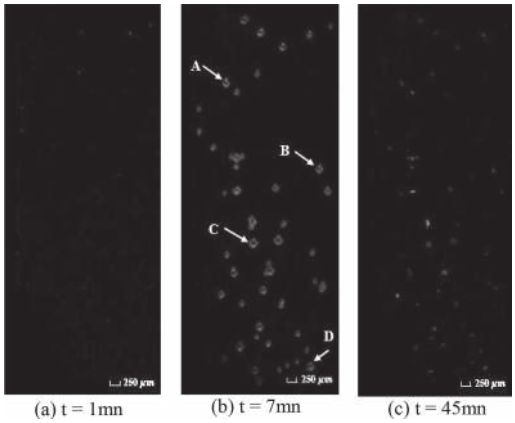

Figure 4. Damage morphology of a sample submitted to P_{sat} = 9 MPa and $\dot{P}$ = 2.5 MPa/min (all images were taken after the onset of the first cavity).

which was fast enough to get out of the sample without damage.

Results in the present EPDM confirmed Jaravel's observations in a silicone rubber (Jaravel et al. 2011), i.e. t_{cav} decreased as the decompression rate increased or increased with the saturation pressure. Dependence on these two parameters was shown to be non-linear.

3.2 *Evolution of the cavity fields*

Pictures in Figure 4 were taken at different times after the onset of the first cavity. Other cavities appeared at different times and randomly throughout the volume of the sample. Figures 5 and 6 display the evolution of the number of cavities per mm² and the average diameter respectively, for both sample geometry. First, cavities appeared randomly through the sample with a 25 µm diameter (detection threshold) and then each cavity grew with its own kinetic between t_{cav} and 11 min after the onset of damage; at this time, the number of cavities nucleated reached its maximum. At the end of the inflation step, the biggest cavities exhibited a diameter about 300 µm. Most cavities then deflated and seemed to close. However, largest cavities and crack remained visible even 2 hours after decompression (Figure 4d). In these decompression conditions, there was always less than one cavity per mm² on average.

Curves in Figures 5 and 6 showed that the number of cavities and average diameter did not depend on the sample geometry, suggesting that rectangular samples were large enough to capture representative fields for these two parameters.

To highlight the inflation/deflation kinetics of single cavities, the diameter of 4 cavities randomly selected in the middle part of the sample (see in Figure 4b) was plotted all along their life cycle in Figure 7. All curves were plotted as a function of the time elapsed since the onset of the first cavity. The inflation kinetics was the same for all cavities. Deflation started at the same time but with slightly different kinetics.

Work is in progress to confront these experimental results to numerical simulations of single cavity inflation and deflation by Finite Element Method.

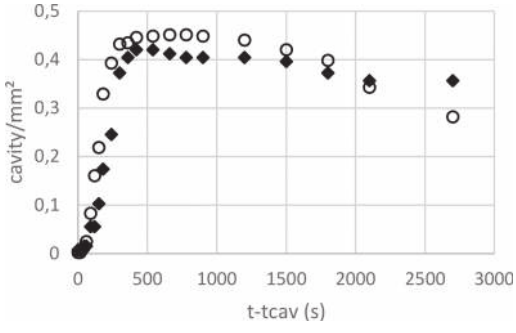

Figure 5. Evolution of cavities number since the onset of damage: square sample (circles), rectangular sample (lozenges).

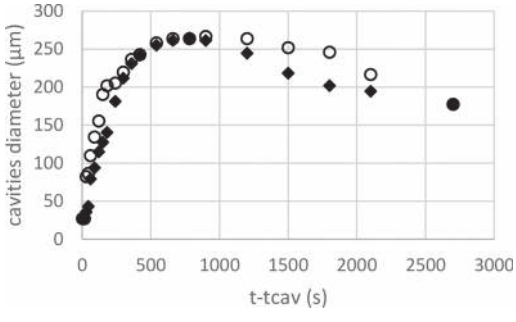

Figure 6. Evolution of the average of cavities since the onset of damage: square sample (circles), rectangular sample (lozenges).

3.3 *Spatial distribution*

Damage morphology analysis at the cavity field scale was completed by considering the spatial distribution and its evolution with time. Such information is important for further purpose of predictive modeling. The concept of REV for instance is crucial for multi-scale modeling or microstructure numerical calculations. It is then necessary to define more precisely REV dimensions, the number of cavities to be introduced and their distribution over the computed volume. To achieve this, covariograms were built up along the horizontal and vertical directions of processed pictures. Figure 8 and Figure 9 show the time evolution of one of the

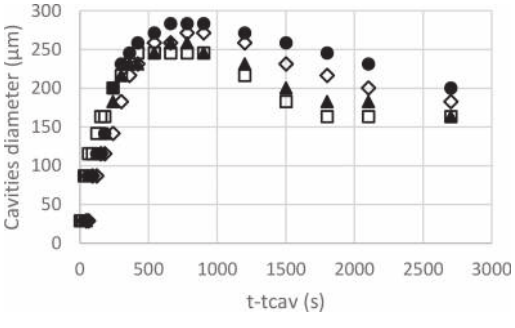

Figure 7. Evolution of the diameter of some cavities tracked during the cavitation damage: cavity A (triangles), cavity B (lozenges), cavity C (circles), cavity D (square).

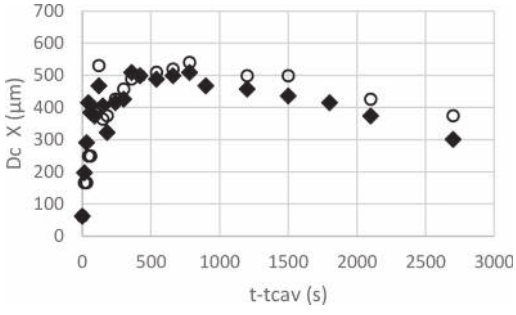

Figure 8. Evolution of the correlation length along x axis since the onset of damage: square sample (circles), rectangular sample (lozenges).

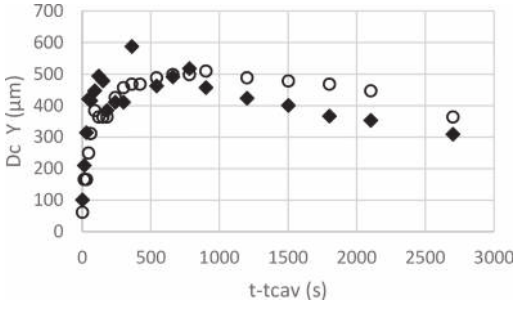

Figure 9. Evolution of the correlation length along y axis since the onset of damage: square sample (circles), rectangular sample (lozenges).

parameters extracted from covariograms, i.e. the correlation length along the vertical (x) and horizontal (y) direction respectively.

First, it could be noted that curves were almost identical for both sample geometry, regardless the direction of the covariogram, meaning that no anisotropy was introduced at the morphological REV scale by the rectangular shape.

Secondly, by comparing Figure 5 and Figure 6, i.e. the horizontal and vertical direction, it could be deduced that the correlation length was the same in both directions. All along the test, the morphological REV resulted isotropic. D_c along axis x and y was equal to 500 µm (measured at 8 mn, when cavities nucleated reach its maximum). Also, it meant that the REV would be a square with size depend on time as follows:

– REV was less than 50 µm in the early stages of nucleation
– REV was maximal (approximately 500 µm) when the number of bubbles was maximal.

The statistical distribution more or less evolved with the average size of the cavity. In such decompression conditions, the nucleation of new cavities did not affect the statistics of the existing cavity field. It was shown that it was not the case any more for more severe decompression conditions.

The distance D_r between cavities appeared weak and relatively independent on time as represented in Figure 10. This distance was more than 1500 µm at the first step of nucleation (few cavities but distant from each other) and became less than 10 µm in advanced stages of damage (many cavities but very close to each other). Interaction between cavities is then expected to be strong and important to take account. However, Figure 10 shows that the distance between cavities along x axis was less than that along y ($D_r(x)$ = 5 µm and $D_r(y)$ = 10 µm at 8 min after the end of decompression).

Figure 11 focuses on the macroscopic scale by comparing the asymptote value of covariograms along the horizontal and vertical axis.

It could be pointed out that isotropy depended on time. Between the onset of cavitation and 4 min after, asymptotes x and y almost overlapped, meaning that the statistical distribution

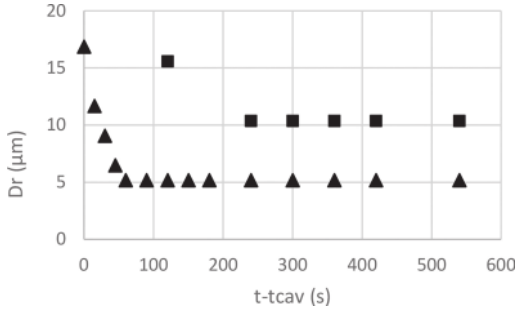

Figure 10. Zoom on the evolution of the repulsion distance with rectangular sample since onset of damage along x axis (triangle) and y axis (square).

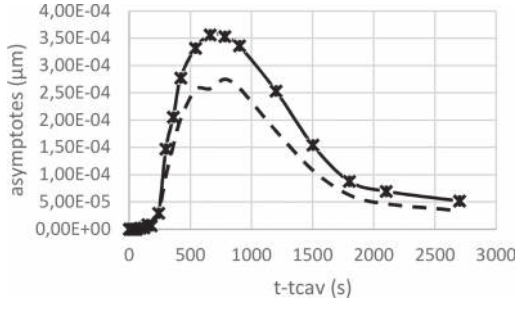

Figure 11. Evolution of the asymptotes since onset of damage along x axis (dash with cross point) and y axis (dot line).

was macroscopically isotropic in this time period. In fact, there were not enough cavities (less than about 30 cavities) to macroscopically disturb the spatial distribution of cavities. During the following stage, the increase of cavities number added to the fact that each cavity had its own growth kinetics, made the statistical distribution macroscopically anisotropic: asymptote x became larger than asymptote y with a maximum difference of 40%. It meant that the probability of encountering another cavity along x axis was greater than along y axis. Finally, isotropy was recovered later, during the last stage corresponding to the deflation of cavities and to the closure of some of them.

Same results were obtained in the square samples, showing that rectangular samples were large enough to be representative of experiments.

4 CONCLUSION

The aim of this study was to provide information about the statistics of cavity fields nucleated in an EPDM rubber upon decompression, after hydrogen exposure. Analysis was based on covariogram method applied to successive pictures taken all along decompression tests. The evolution of the cavities number and its average size was shown to depend on time. Covariogram parameters were shown to be time-dependent too.

Two sample geometries (rectangle and square) were tested. Comparison showed that rectangular samples were large enough to capture representative statistical parameters.

At the macroscopic scale, the distribution was shown to be isotropic and homogeneous during the first nucleation stage and at the end of deflation stage (a few tens of cavities in each case). In between, anisotropy appears with a maximum difference about 40% between the vertical and horizontal directions.

At the cavity scale, the onset of new cavities did not affect the statistical distribution of cavities in the reported decompression conditions. REV was found to be isotropic all along the test, with a size almost following the average size of cavities. Consistently, the inflation/deflation kinetics of single cavities randomly picked up in the field was shown to be almost the same.

From another test campaign (not reported in this paper) performed to quantify the effect of decompression conditions, it could be shown that the statistical distribution of cavities depended strongly on the time onset of cavitation (during decompression or after the end of decompression).

ACKNOWLEDGEMENTS

Authors would like to gratefully acknowledge Pr. Nishimura, Dr. Fujiwara and Dr. Ono, from Hydrogenius Laboratory at Kyushu University, for fruitful discussion. French Ministery for Education and Research is also acknowledged for granting O. Kane-Diallo's PhD.

This work pertains to the French Government program "Investissements d'Avenir" (LABEX INTERACTIFS, reference ANR-11-LABX-0017-01).

REFERENCES

Bez, J., Rivoirard, J. & Poulard. (1995). Covariogamm: a structural tool. *Second forum halieumeric, Information analysis*, Nantes.

Briscoe, B.J., Savvas, T. & Kelly, C.T. (1994). Explosive decompression failure of rubber: a review of the origins of pneumatic stress induced rupture in elastomer. *Rubber Chemistry and Technology* 67:384–416.

Busse, W.F. (1938). Physics of rubber as related to the automobile. *J. Appl. Phys*. 9:438–51.

Castagnet, S. & Gandidier, J.C. (2010). Mechanical testing of polymers into pressurized hydrogen: tension, creep and ductile fracture. *Exp. Mech*. DOI 10.1007/s11340-011-9884-1.

Cressi (1991). Spatial statistics. *Wiley and Sons*, New York.

Gent, A. & Lindley P.B. (1959). Internal rupture of bonded rubber cylinders in tension. *Proc Royal Soc A: Math Phys Eng Sci 1959* A249:195–205.

Jaravel, J. & Castagnet, S. (2011). On key parameters influencing cavitation damage upon fast decompression in a hydrogen saturated elastomer. *Polymer Testing* 30:811–818.

Jaravel, J., Castagnet, S., Grandidier, J.C. & Gueguen, M. (2013). *Int. Journal of Solids and Structures* 50: 1314–1324.

Lindsey, G.H. (1967). Triaxial fracture studies. *Journal of Applied Physics* 38:4843–4852.

Nait-Ali, A., Kane-diallo, O. & Castagnet, S. (2015). Catching the time evolution of microstructure morphology from dynamic covariograms. *To be published in Comptes rendus-Mecanique* doi10.1016/j.crme.2015.02.005.

Stewart, C.W. (1970). Nucleation and growth of bubbles in elastomers. *Journal of Polymer Science Part a-2-Polymer Physics* 8, 937-&.

Yamabe, J., Nakao, M., Fujiwara, H. & Nishimura, S. (2008). Blister fracture of rubbers for O-ring exposed to high pressure hydrogen gas. *In: Hydrogen conference, Jackson Lake Lodge*, USA.

Yamabe, J., Nishimura, S. (2011). Crack growth behavior of sealing rubber under static strain in high-pressure hydrogen gas. *J. Solid Mech. Mater. Eng.* 5:690–701.